Photosynthesis Research
https://doi.org/10.1007/s11120-022-00993-w

ORIGINAL ARTICLE

# Drop-casted Photosystem I/cytochrome c multilayer films for biohybrid solar energy conversion

**Long Than[1] · Kody D. Wolfe[2] · David E. Cliffel[3] · G. Kane Jennings[1]**

Received: 12 July 2022 / Accepted: 3 December 2022


## Abstract

One of the main barriers to making efficient Photosystem I-based biohybrid solar cells is the need for an electrochemical pathway to facilitate electron transfer between the $P_{700}$ reaction center of Photosystem I and an electrode. To this end, nature provides inspiration in the form of cytochrome $c_6$, a natural electron donor to the $P_{700}$ site. Its natural ability to access the $P_{700}$ binding pocket and reduce the reaction center can be mimicked by employing cytochrome c, which has a similar protein structure and redox chemistry while also being compatible with a variety of electrode surfaces. Previous research has incorporated cytochrome c to improve the photocurrent generation of Photosystem I using time consuming and/or specialized electrode preparation. While those methods lead to high protein areal density, in this work we use the quick and facile vacuum-assisted drop-casting technique to construct a Photosystem I/cytochrome c photoactive composite film with micron-scale thickness. We demonstrate that this simple fabrication technique can result in high cytochrome c loading and improvement in cathodic photocurrent over a drop-casted Photosystem I film without cytochrome c. In addition, we analyze the behavior of the cytochrome c/Photosystem I system at varying applied potentials to show that the improvement in performance can be attributed to enhancement of the electron transfer rate to $P_{700}$ sites and therefore the PSI turnover rate within the composite film.

**Keywords** Biohybrid energy conversion · Photosystem I · Cytochrome c · Drop-casting · Electrochemistry · Redox proteins · Thin films · Biohybrid materials · Solar energy

## Introduction

Finding affordable and environmentally friendly alternatives to conventional solar energy conversion technologies is particularly important because of their current reliance on rare earth metals and/or energy-intensive manufacturing processes. Biohybrid photocatalytic devices based on Photosystem I (PSI) have the potential to fill that niche due to the remarkable electrochemical properties of this photosynthetic protein complex, such as a near perfect internal quantum efficiency (Golbeck and Bryant 1991) and a reduction potential among the lowest exhibited in nature (−0.59 V vs. SHE) (Nelson and Ben-Shem 2005). In addition, PSI's abundance, robustness, and ease of isolation are favorable characteristics from a manufacturability perspective.

An ongoing challenge to improving the solar conversion efficiency of PSI-based biohybrid devices is to design an electron transfer pathway that can access both the PSI reaction centers and the electrode. In nature, light absorption by PSI causes the excitation of the $P_{700}$ reaction center, a chlorophyll special pair located near the lumenal side of the protein complex (Chitnis 2001). This citation triggers a series of internal electron transfer events that facilitate charge separation and stabilization, ultimately resulting in the oxidation of $P_{700}$ to $P_{700}^{+}$ and the reduction of the terminal reaction center $F_B$, an Fe-S cluster located on the stromal side of the protein, to $F_B^{-}$ (Brettel and Leibl 2001). The $P_{700}^{+}$ site is then reduced by either plastocyanin or cytochrome $c_6$, and the $F_B^{-}$ site is oxidized by ferredoxin. In biohybrid electrochemical systems, the $P_{700}$ and $F_B$ sites need to interface

✉ G. Kane Jennings
kane.g.jennings@vanderbilt.edu

[1] Department of Chemical and Biomolecular Engineering, Vanderbilt University, Nashville, TN 37235-1604, USA

[2] Interdisciplinary Materials Science and Engineering Program, Vanderbilt University, Nashville, TN 37235-0106, USA

[3] Department of Chemistry, Vanderbilt University, Nashville, TN 37235-1822, USA

Published online: 24 December 2022

directly with two different electrode surfaces that facilitate direct electron transfer, or react with electrochemical mediator species that shuttle electrons between the PSI reaction centers and the electrode(s). Some approaches that have succeeded in the past include using small molecule mediators (Ciesielski et al. 2010; Chen et al. 2013; Teodor et al. 2021), assembly with redox polymers (Badura et al. 2011; Kothe et al. 2014; Dervishogullari et al. 2018) or conductive polymers (Gizzie et al. 2015; Wolfe et al. 2021), and wiring to metal nanoparticles (Grimme et al. 2008; Zhu et al. 2020). For favorable electron transfer kinetics to occur, two common themes among these approaches are that the species interfacing with PSI reaction centers must: (1) be able to access the reaction centers of PSI, especially the $P_{700}$ site, which is situated within a binding pocket, and (2) have favorable energetics (i.e., redox potentials) that are compatible with those of the reaction centers. Based on these considerations, one mediator that has received considerable interest as a redox partner with PSI is cytochrome c (cyt c), a heme-containing redox-active protein. Cyt c belongs to the same protein family as cytochrome $c_6$, the natural electron donor to the $P_{700}$ site of PSI in thermophilic photosynthetic bacteria (Sarauli et al. 2010; Stieger et al. 2016a). Their similarities allow the two cytochromes to form similar docking sites with PSI–primarily at the lumenal side of the protein complex and clustered near the $P_{700}$ site, therefore resulting in a short electron transfer distance (Kölsch et al. 2018). Thus, cyt c has the potential to act as a fast electron relay between the relatively inaccessible $P_{700}$ site and the electrode. Furthermore, cyt c is well-studied in the field of bioelectrochemistry due to its fast electron transfer kinetics with a variety of electrode surfaces (Scheller et al. 1999; Chen et al. 2002; Ge and Lisdat 2002; López-Bernabeu et al. 2017; Aghamiri et al. 2018). Cyt c has also shown success in acting as an interface between electrodes and redox enzymes, primarily for the construction of electrochemical biosensors (Balkenhohl et al. 2008; Spricigo et al. 2009; Feifel et al. 2012).

Indeed, the combination of cyt c and PSI has already been investigated in a variety of electrode types and architectures. Efrati et al. were the first to report the co-immobilization of cyt c and PSI for photo-bioelectrochemistry, specifically within a PSI/cyt c/PSII composite film supported by a polyvinyl pyridine/methyl pyridinium matrix (Efrati et al. 2013). Stieger et al. investigated the self-assembly of cyt c and PSI composite films on planar gold modified with negatively charged thiol-based self-assembled monolayers (Stieger et al. 2014, 2016a), showing that cyt c could facilitate electron transfer between the specialized electrode surface and the $P_{700}$ site to enhance photocurrent in the cathodic direction. Furthermore, the layer-by-layer deposition technique was employed to construct three-dimensional photoactive films with higher photocurrent densities, showing that not only can immobilized cyt c shuttle electrons toward PSI adsorbed directly on the electrode surface, but it can also facilitate long-distance electron transfer to PSI immobilized further away that would otherwise be inaccessible via direct electron transfer. Similarly, photoactive biohybrid electrodes incorporating cyt c and PSI have been constructed from porous electrode materials such as mesoporous indium tin oxide (Stieger et al. 2016b; Ciornii et al. 2019) or reduced graphene oxide on glassy carbon (Morlock et al. 2021). The porous architecture allows for increased protein loading density per geometric surface area, increasing photocurrent density compared to a 2D electrode surface; furthermore, the areal density of cyt c and PSI can be increased by increasing the number of electrode layers, resulting in thicker porous layers with more surface area for protein adsorption. These studies demonstrate that the photocurrent performance enhancement by cyt c is scalable by moving toward a 3D photoactive film architecture. However, improving photocurrent density via these strategies is limited by the difficulty of producing thicker films, whether by the time-consuming layer-by-layer deposition process or by successive depositions of porous electrode material.

A simpler method to produce photoactive layers incorporating PSI and cyt c with three-dimensional architecture is needed. The goal of this work is to employ the vacuum-assisted drop-casting technique, previously demonstrated by our group (Ciesielski et al. 2010), to construct thick films containing both proteins–as well as Nafion as a stabilizing layer–in a quick and facile manner, resulting in a biophotocathode with rapid assembly time, little to no material loss during construction, and micron-scale film thickness. We show that the drop-casted film is capable of physically retaining electronically accessible cyt c, not only at the electrode-film interface, but also within the three-dimensional film architecture; furthermore, the incorporation of cyt c improves the electron transfer kinetics between PSI and the electrode to enhance cathodic photocurrent density.

## Experimental method

### Materials

Mercaptoundecanol (MU) and mercaptoundecanoic acid (MUA) were obtained from Sigma-Aldrich. Perfluorosulfonic acid-polytetrafluoroethylene copolymer (Nafion) was obtained as a 5 wt% solution in 50:50 water:propanol (Alfa Aesar) and was diluted by a factor of 100 in deionized water to obtain a 0.05 wt% Nafion solution. Methyl viologen hydrate (98%) was obtained from Acros Organics.

Lyophilized equine heart cytochrome c (cyt c) was obtained from Sigma-Aldrich and was dissolved in 5 mM phosphate buffer (pH 7) to form a 120 µM solution.

Lyophilized cyt c was stored at −20 °C until dissolution; cyt c solutions were stored at −20 °C for up to 6 months, and once thawed, were stored at 2 °C and used within 3 days.

## PSI preparation

PSI was extracted from commercial baby spinach using a previously described procedure (Shiozawa et al. 1974; Baba et al. 1996; Wolfe et al. 2021). In short, the thylakoid membrane containing the protein was extracted via mechanical maceration, filtration, and centrifugation. The surfactant Triton X-100 (Sigma) was then used to lyse the membrane and stabilize the protein in aqueous solution. Another centrifugation step was performed to isolate PSI in the supernatant. Ion affinity chromatography was used to purify the PSI solution. The column effluent had an approximate concentration of 0.5 mg PSI/mL in 200 mM phosphate buffer (pH 7) containing 0.5 g $L^{-1}$ Triton X-100. Finally, the solution was dialyzed as 1 mL aliquots in 2000 mL of de-ionized water for 24 h using 10,000 MWCO dialysis tubing (Spectrapore), reducing the concentrations of the phosphate buffer and Triton X-100 to 0.1 mM and 0.25 mg $L^{-1}$, respectively. PSI was stored at − 80 °C in 1 mL aliquots until dialysis, after which the dialyzed solution was stored in the refrigerator (~2 °C) for up to two weeks.

## Electrode preparation

Gold disk electrodes (2 mm diameter) were used for electrochemical analyses. The electrodes were cleaned by polishing with diamond paste (0.1 micron, UBS, Electron Microscopy Sciences), sonicating in ethanol, then cycling between 1.0 and −1.0 V in 2 mM sulfuric acid. The electrode was then incubated in an ethanolic solution of 5 mM mercaptoundecanol and mercaptoundecanoic acid at a 3:1 ratio (MU:MUA) for at least 48 h, then rinsed with ethanol followed by water, and dried with nitrogen. This SAM composition was chosen to maximize the activity of adsorbed cyt c (Ge and Lisdat 2002).

Gold substrates used for other characterization techniques were prepared by thermally evaporating a 125 nm thick gold layer onto a chromium-primed silicon (100) support, as described previously (Kincaid et al. 2006). The gold-coated wafers were cut into 1.0 cm × 2.0 cm samples, cleaned with three alternating rinses of ethanol and deionized water, dried with nitrogen, and incubated in an MU:MUA solution for at least 48 h as described above. Afterward, the electrodes were rinsed with ethanol followed by water, dried with nitrogen, and masked with hole-punched electrochemical sample masks to limit the exposed surface area to 0.28 $cm^2$.

## Film assembly via vacuum-assisted drop-casting

The cyt c/PSI/Nafion film was prepared by drop-casting and drying cyt c, followed by PSI, and finally Nafion onto the cleaned gold disk electrode modified with the MU:MUA SAM. For each drop-casting step, 5 µL of the drop-casting solution was pipetted onto the substrate; then, the sample was dried in a vacuum chamber at 30 mTorr for ~5 min. For films prepared on the silicon-supported gold substrate, 50 µL of each drop-casting solution was pipetted, and the sample was dried for ~20 min. The drop-casting and drying steps were then repeated for each component in the film (Fig. 1). The average profilometric thickness of the resulting film after rinsing is 0.9 µm with a surface roughness of 0.2 µm. The other films investigated (cyt c/PSI, cyt c/Nafion, cyt c, and PSI) were similarly prepared by drop-casting the appropriate solutions in the order described (cyt c then PSI for cyt c/PSI, etc.)

## Contact profilometry

Profilometry was performed with a Veeco Dektak 150 stylus profilometer. The scan force was 6.5 mg with a scan rate of 16.7 µm $s^{-1}$. The sample was prepared by etching a line across the film using forceps to reveal the gold substrate,

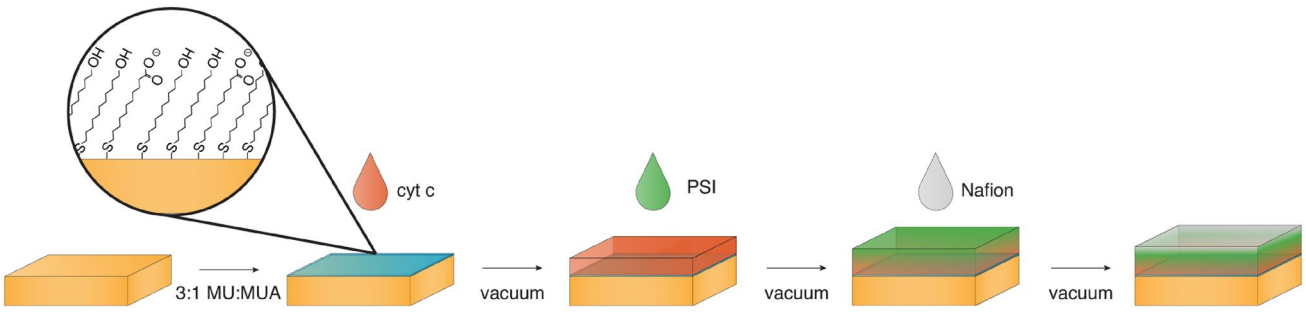


**Fig. 1** Schematic of the drop-casting procedure to form a cyt c/PSI/Nafion film, including surface modification of the gold electrode with a MU:MUA self-assembled monolayer

then performing a line-scan perpendicular to the etched line. The film thickness was measured using the exposed gold substrate as the reference height. The average thickness of each sample was calculated from line scans across three different areas of the sample.

### Reflectance UV–Vis spectroscopy

Ultraviolet visible (UV-vis) spectroscopy was performed using a Varian Cary 5000 UV–VIS-NIR spectrophotometer operating in dual beam mode with a specular reflectance accessory. The scan range was 300–1000 nm, and the scan rate was 300 nm $min^{-1}$. A gold substrate with a MU:MUA SAM was used as the reference sample.

### Fourier transform infrared spectroscopy

Attenuated total reflectance Fourier transform infrared (ATR-FTIR) spectroscopy was performed using a Thermo Nicolet 6700 FT-IR spectrometer equipped with a liquid-nitrogen-cooled mercury-cadmium-telluride (MCT) detector and Smart iTR ATR attachment with a diamond crystal plate. The spectra were collected within the 4000–700 $cm^{-1}$ range over 256 scans.

### Electrochemical characterization

All electrochemical measurements were performed with a CH Instruments CHI660a potentiostat equipped with a Faraday cage. The modified gold substrate was used as the working electrode, a platinum mesh as the counter electrode, and Ag/AgCl as the reference electrode. The electrolyte solution was 5 mM phosphate buffer (pH 7) unless otherwise specified. Cyclic voltammetry (CV) experiments were performed at a scan rate of 50 mV $s^{-1}$ between 300 and −300 mV vs. Ag/AgCl. Unless otherwise stated, measurements of CV curve characteristics were taken during the 3rd cycle. Photochronoamperometric experiments were performed at open circuit potential (OCP), −200 mV vs. OCP, and 200 mV vs. OCP. In each experiment, the electrochemical cell was allowed to equilibrate at the chosen applied potential for 120 s before the sample was illuminated with a 100 mW $cm^{-2}$ white light source (Leica KL 2500 LCD) for 60 s, followed by 60 s in the dark. Outlier results ($\alpha = 0.05$) compared to the set of results from identically prepared samples were identified via Grubbs' test and excluded from statistical analysis.

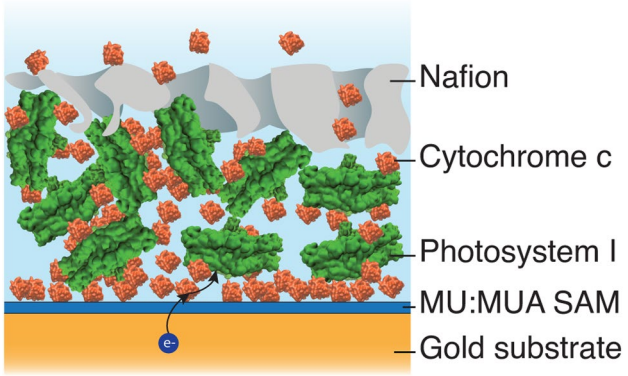


**Fig. 2** Schematic of the cyt c/PSI/Nafion photoactive film

## Results & discussion

### Cyt c retention

The drop-casting method allows for the rapid deposition of all the solute material in the drop of solution onto the electrode surface to achieve micron-scale protein films. The resulting film is susceptible to partial dissolution when re-exposed to an aqueous environment. Although this effect is minor for PSI due to its hydrophobicity, cyt c is highly soluble and therefore forms an unstable film. To increase the stability of cyt c, a mixed film approach is suitable as cyt c demonstrates the ability to complex with PSI based on electrostatic attraction between oppositely charged amino acid side chains (Kölsch et al. 2018). The desired film architecture was achieved by first depositing a cyt c film, allowing for an adsorbed cyt c monolayer to form at the electrode surface uncontested by PSI adsorption, followed by a PSI film. The bulk of the cyt c film redissolves as the PSI solution is added, and cyt c-PSI complexes are formed before the solution is evaporated to form the composite film (Stieger et al. 2016a) (Fig. 2). Finally, Nafion is drop-casted to form a protective layer and limit cyt c dissolution; the polymer contains negatively charged sulfonate functional groups that bind to cyt c, which is positively charged at neutral pH (Stieger et al. 2014). Nafion also forms ion channels when hydrated, allowing mediator species in solution to access the protein film (Kraytsberg and Ein-Eli 2014). Furthermore, Nafion is synergistic with PSI as it can also interact electrostatically with the protein complex to improve retention near the surface, while being transparent to the visible wavelengths of light that PSI absorbs to perform its photocatalytic function (Baker et al. 2014).

Cyclic voltammetry is the conventional analytical technique used to probe the activity of surface-bound cyt c by monitoring the Faradaic peak associated with the reduction and oxidation of the heme group. We used the technique

to investigate the stability of cyt c within the drop-casted films, showing that the Faradaic peak intensity reaches the order of ~10 μA/cm$^2$ during the initial scan but trends toward a much smaller intensity over time (Fig. SI.1 in Online Resource 1). This behavior can be attributed to the initial high loading of cyt c within the film, most of which is weakly bound and rapidly diffuses into the solution. After rinsing the electrode to accelerate the removal of weakly bound cyt c, the resulting peak intensity is consistent over multiple CV cycles. This indicates that the remaining cyt c is strongly adsorbed to the SAM and/or entrapped by the surrounding polymer and PSI to allow for stable redox activity.

We observed that the stable level of cyt c peak intensity is highly influenced by the film composition. Bare cyt c drop-casted on the SAM resulted in the lowest peak intensity after rinsing, followed by cyt c/Nafion, cyt c/PSI, and cyt c/PSI/Nafion in increasing order (Fig. 3). Furthermore, the $E_{1/2}$ of cyt c also shifts positively in the presence of PSI, which is caused by a shift in the local environment surrounding cyt c and thus indicates interactions between PSI and cyt c.

The improvement in cyt c activity after drop-casting PSI and/or Nafion can be attributed to the formation of a stable matrix with surface charges offering a favorable electrostatic environment for cyt c retention. Within this film, the surface area available for interaction with cyt c is greater than that for the planar SAM surface, leading to higher cyt c retention.

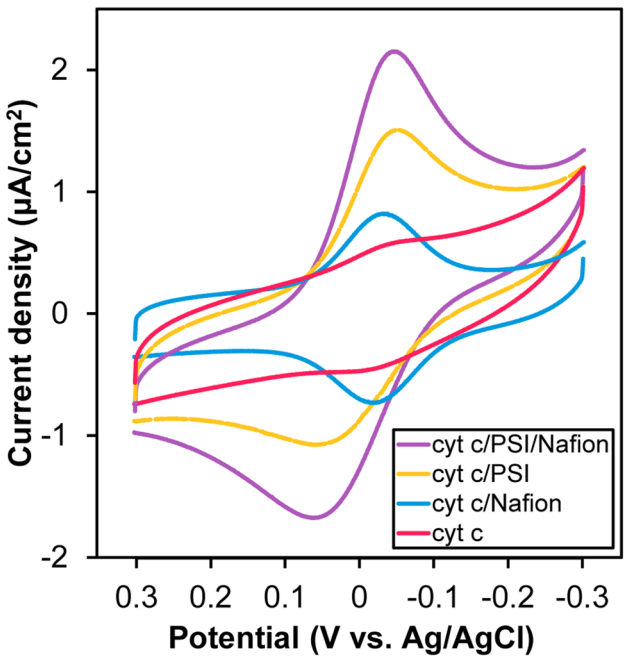


**Fig. 3** Electrochemical behavior of cyt c, cyt c/Nafion, cyt c/PSI, and cyt c/PSI/Nafion drop-casted multilayer films after being rinsed to remove weakly adsorbed material. Cyclic voltammograms were obtained by cycling between 300 and −300 mV at 50 mV/s in 5 mM phosphate buffer (pH 7)

Both PSI and Nafion also contribute to cyt c retention by inhibiting diffusion of cyt c from the film. The insolubility of both dialyzed PSI and Nafion in aqueous solution allows these components to form a film that is mechanically stable within which cyt c is retained with improved stability.

To gain a physical perspective on the level of cyt c retention within the film, we assumed that the cyt c redox reaction is limited by surface kinetics, a condition that results in a Gaussian peak shape in the CV. The cyt c adsorption density can therefore be estimated based on the area of the Gaussian peak. The estimation is valid for systems where only surface-adsorbed cyt c participates in redox reactions and is less accurate for systems where cyt c participates as a diffusing mediator, in which case mass transfer kinetics would influence the shape of the CV curve. Data on the estimated adsorption density and other extracted CV parameters are tabulated in Table 1 and in Fig. SI.2 in Online Resource 1.

In the case of drop-casted cyt c, only the negatively charged SAM is present to interact with cyt c; thus, only a (sub)monolayer of cyt c can be retained at the surface while the rest of the film is dissolved. The estimated adsorption density of 1.9 pmol cyt c/cm$^2$ as well as the small peak separation (43 ± 3 mV) between the oxidation and reduction peaks confirm that a partial monolayer of cyt c has been retained, compared to the theoretical maximum adsorption density of 15 pmol/cm$^2$ assuming perfect packing in a planar configuration (Song et al. 1993).

Compared to the drop-casted cyt c film, drop-casting a layer of Nafion after cyt c (cyt c/Nafion) increases the adsorption density to 16 ± 2 pmol cyt c/cm$^2$ while retaining small peak separation and a similar $E_{1/2}$, indicating that redox activity primarily comes from surface-adsorbed cyt c. However, this improvement in cyt c adsorption is minor in comparison to the cyt c/PSI film, which retains 31 ± 14 pmol cyt c/cm$^2$. The presence of PSI also dramatically increases the peak separation and peak width; we believe that this is caused by a large proportion of electroactive cyt c acting as a mobile redox species entrapped within the film rather than a surface-adsorbed species. This argument is supported by a study on the effect of scan rate on peak intensity (Fig. SI.3 in Online Resource 1), which shows a strong linear

**Table 1** Summary of multilayer film characteristics measured via cyclic voltammetry

| | Areal density (pmol/cm$^2$) | $E_{1/2}$ (mV) | Peak separation (mV) |
|---|---|---|---|
| cyt c | 1.9 ± 0.2 | −23 ± 30 | 43 ± 3 |
| cyt c/Nafion | 16 ± 2 | −28 ± 2 | 14 ± 2 |
| cyt c/PSI | 31 ± 14 | 9 ± 7 | 119 ± 22 |
| cyt c/PSI/Nafion | 33 ± 15 | −6 ± 10 | 77 ± 32 |

correlation between the square root of scan rate and peak intensity in accordance with the Randles–Sevcik equation. This dependence on scan rate shows that the PSI film retains cyt c throughout its volume via electrostatic interaction while maintaining cyt c mobility to allow for redox activity; thus, the local concentration of cyt c is high despite the lack of cyt c in the bulk solution, and the amount of cyt c available to react is able to exceed the monolayer limit. On the other hand, the cyt c/Nafion film cannot exceed the monolayer limit for cyt c activity because of the much stronger interaction between cyt c and Nafion (Hahn et al. 1990), which immobilizes cyt c within the Nafion film and prevents its diffusion to the surface. Therefore, only cyt c directly adsorbed on the surface can participate in redox reactions.

One drawback of the cyt c/PSI film is that the cyt c adsorption density is less consistent, albeit improved, compared to either the cyt c or cyt c/Nafion films. This may be due to the inherent variability of the drop-casting process. For example, the coffee-ring effect and aggregation of PSI are known issues for drop-casted PSI films, and can allow for the formation of channels and regions of thinner film from which cyt c escapes more easily via diffusion.

The composite film combining cyt c, PSI, and Nafion (cyt c/PSI/Nafion) exhibits a similar CV as the cyt c/PSI film, featuring a cyt c areal density of $33 \pm 15$ pmol/cm$^2$ that is similarly inconsistent and high peak separation suggesting that electronically accessible cyt c is found primarily within the PSI/Nafion film instead of the electrode surface. The presence of Nafion was confirmed via ATR-FTIR (Fig. SI.4 in Online Resource 1). Therefore, the similarities between cyt c/PSI/Nafion and cyt c/PSI in terms of electrochemical behavior and cyt c retention may be due to the inability of the Nafion layer to penetrate deep into the PSI layer and affect the local environment near the electrode surface. The inclusion of PSI in cyt c/PSI/Nafion (and cyt c/PSI) may also cause the film to be more disordered compared to cyt c/Nafion, disrupting the strong ionic interaction between Nafion and cyt c and increasing cyt c mobility despite the presence of Nafion.

The capability of the films to retain cyt c after rinsing was also investigated via reflectance UV–vis spectroscopy. When comparing the spectra for unrinsed and rinsed cyt c/PSI/Nafion, the only difference was a small decrease in the intensity of the Q-band at 526 nm attributed to the cyt c heme porphyrin ring (Fig. 4) (Oellerich et al. 2002). This result suggests that cyt c is retained at a much higher level than the picomole level that is detectable via CV, but remains mostly electronically inaccessible due to the large distance from the electrode and slow diffusion through the PSI/Nafion environment.

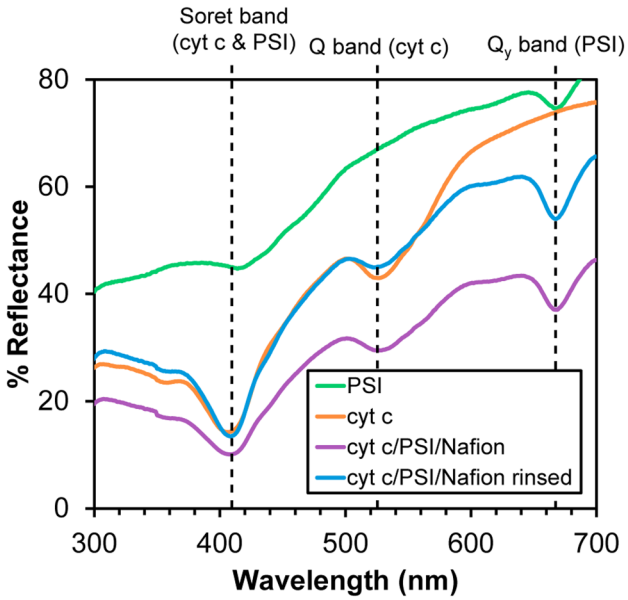


**Fig. 4** Reflectance UV–vis spectra of drop-casted PSI, drop-casted cyt c, and cyt c/PSI/Nafion films between 300 and 700 nm. Spectrum of cyt c/PSI/Nafion taken after rinsing shows retention of film material

## Photochronoamperometric properties

The photoactivity of PSI/Nafion and cyt c/PSI/Nafion films was investigated via photochronoamperometry (PCA) at open circuit potential (OCP) as well as positive and negative biases (+200 mV and −200 mV vs. OCP, respectively) (Fig. 5a). These varying biases affect the electron transfer kinetics within the system, therefore causing different PCA results. The behaviors from each condition are described and contrasted in the following sections (Open Circuit Potential, Negative Bias, and Positive Bias):

### Open circuit potential

At OCP, electron transfer in a system without cyt c (i.e., the PSI/Nafion control) is mediated by oxygen at the $F_B^-$ site and reduced oxygen species (ROS) at the $P_{700}^+$ site. During illumination, oxygen reduction by $F_B^-$ occurs more quickly than ROS oxidation by $P_{700}^+$, resulting in the net production of reduced species; therefore, a small anodic photocurrent is produced by the negative shift in the equilibrium potential of the solution. This photocurrent is limited by the low concentration of dissolved oxygen and the diffusion rate of ROS and $O_2$.

On the other hand, the cyt c/PSI/Nafion system features cyt c as a fast electron donor to the $P_{700}$ site, changing the mechanism of photocurrent generation. The film produces cathodic photocurrent at OCP due to the fast kinetics of cyt c

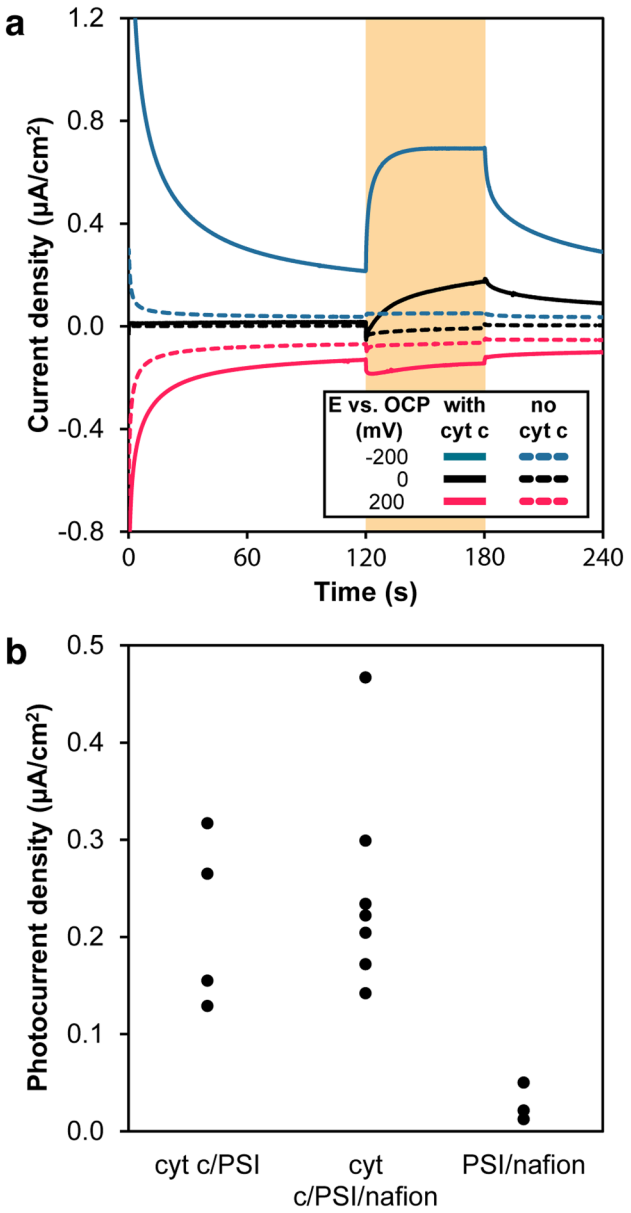


**Fig. 5** **a** Photochronoamperometry experiments of cyt c/PSI/Nafion (solid lines) and PSI/Nafion (dashed lines) in 5 mM phosphate buffer. Experiments were performed at OCP (black) and −200 mV (blue) +200 mV (red) applied potentials relative to OCP. The sample was illuminated between 120 and 180 s. OCPs were as follows: Cyt c/PSI: 86 ± 31 mV (vs Ag/AgCl); Cyt c/PSI/Nafion: 75 ± 26 mV; PSI/Nafion: 121 ± 11 mV. **b** Photocurrent density in 5 mM phosphate buffer of cyt c/PSI, cyt c/PSI/Nafion, and PSI/Nafion multilayer films, recorded at −200 mV vs. the OCP of the sample

at the $P_{700}^+$ site. During illumination, light-catalyzed oxidation of the $P_{700}$ site occurs, and cyt c is quickly oxidized by $P_{700}^+$, resulting in the net production of oxidized cyt c near the electrode and therefore cathodic photocurrent according to the Nernst equation. $F_B^-$ continues to donate electrons to oxygen even when cyt c is present, as cyt c is not a natural electron acceptor for the $F_B$ site based on the scarcity of binding sites on the stromal side of the protein complex as compared to the lumenal side (Kölsch et al. 2018).

The rounded square shape of the cyt c/PSI/Nafion photocurrent curve at OCP is indicative that the output of the film is limited by electron transfer kinetics between cyt c and the electrode surface. The oxidized cyt c concentration–and thus the potential driving force–continues to build up over time until the steady state cathodic photocurrent is achieved, matching the rate at which oxidized cyt c is produced by illuminated PSI.

On the other hand, the PSI/Nafion film features a square-shaped curve due to the diffusion limitation on photocurrent and fast electrode kinetics by ROS. The difference in kinetics between cyt c and ROS also explains the initial anodic spike in the cyt c/PSI/Nafion curve, which occurs due to the relatively fast kinetics of the ROS contributing anodic photocurrent until the buildup of oxidized cyt c becomes the more significant factor.

### Negative bias

The impact of cyt c on cathodic photocurrent is further enhanced when a negative bias is applied. The same electron transfer mechanism as at OCP is observed but with a greater rate of cyt c reduction at the electrode. The negative bias causes the electrode to reduce cyt c even without illumination, which is visualized by the cathodic background current. The rate of cyt c reduction is limited by the diffusion rate of oxidized cyt c and nearly approaches steady state at 120 s into the experiment. When illumination occurs, not only is there a greater concentration of reduced cyt c available to $P_{700}^+$, leading to faster PSI turnover, but the kinetics of cyt c reduction at the electrode is enhanced due to the negative bias. A much smaller cathodic photocurrent is observed in the PSI/Nafion system, resulting from a combination of the oxygen/ROS redox couple and the applied (negative) biasing toward reduction and against oxidation of the mediator species.

Another important feature of the cyt c/PSI/Nafion photocurrent curve, appearing both at OCP and at −200 mV vs. OCP, is the behavior after illumination ends (after 180 s). Here, a significant cathodic current is still observed as compared to the baseline current before illumination. This can be attributed to the excess oxidized cyt c produced by PSI during illumination that combines with the relatively slow cyt c reduction at the electrode, resulting in excess oxidized cyt c persisting even after illumination ends. The amount of excess oxidized cyt c can be estimated by integrating the PCA current at negative bias, assuming that each cyt c protein is only reduced once. This assumption can be made because PSI cannot oxidize cyt c without illumination and therefore cannot replenish the oxidized cyt c consumed by

the residual cathodic current. The amount of cyt c calculated corresponds to the amount in the film that participates in shuttling electrons between the electrode and $P_{700}$ sites. Comparing this value to the previous estimate of cyt c areal density obtained via integration of the CV faradaic peak, similar values were obtained for each sample (Table SI.1 in Online Resource 1). Therefore, we can conclude that most of the cyt c that is electronically accessible (estimated via CV) also participates in reactions with PSI and contributes to the photoactivity of the film (estimated via PCA).

Overall, the positive effect of cyt c on the cathodic photocurrent density of the drop-casted PSI system is clear, with the difference most striking when a negative bias is applied. At −200 mV vs. OCP, the cyt c/PSI/Nafion has an average photocurrent density of $240 \pm 110$ nA/cm$^2$, compared to $31 \pm 19$ nA/cm$^2$ for PSI/Nafion (Fig. 5b). However, there is a large variation in the photocurrent density of the cyt c/PSI/Nafion system, which mirrors the observed variation in cyt c areal density.

#### Positive bias

Applying a positive bias reverses the trends observed at negative bias; cyt c oxidation occurs at the electrode in the dark, leading to a lower concentration of reduced cyt c when illumination begins. This change decreases the rate of electron donation to P700+, which combines with slow cyt c reduction kinetics at the electrode induced by the positive bias to result in a small cathodic photocurrent contribution. The net photocurrent is anodic and similar to that of PSI/Nafion without cyt c, due to heterogeneous oxidation of the excess ROS produced by FB−.

#### Combining cyt c with a fast electron acceptor

In all previous PCA experiments, electron mediation at the $P_{700}$ site was performed by cyt c and/or ROS and at the $F_B$ site by dissolved oxygen. Because the reaction rate at $P_{700}$ is coupled to that of $F_B$, increasing the reaction rate at $F_B$ by introducing a mediator that is more soluble and/or a better electron acceptor for $F_B$ than is oxygen is expected to increase the PSI turnover rate. Methyl viologen ($MV^{2+}$/$MV^{+}$) is one such species that has previously been shown to improve the cathodic photocurrent of a cyt c/PSI assembly (Stieger et al. 2014, 2016a); $MV^{2+}$ is known as a fast electron acceptor at the $F_B$ site, whereas $MV^{+}$ is a poor electron donor to the $P_{700}$ site. As such, we also employed the methyl viologen redox couple to show that the cyt c/PSI/Nafion multilayer film produces greater cathodic photocurrent (at negative bias) when 250 µM $MV^{2+}$ is present (Fig. 6a). This improvement shows that the photocurrent

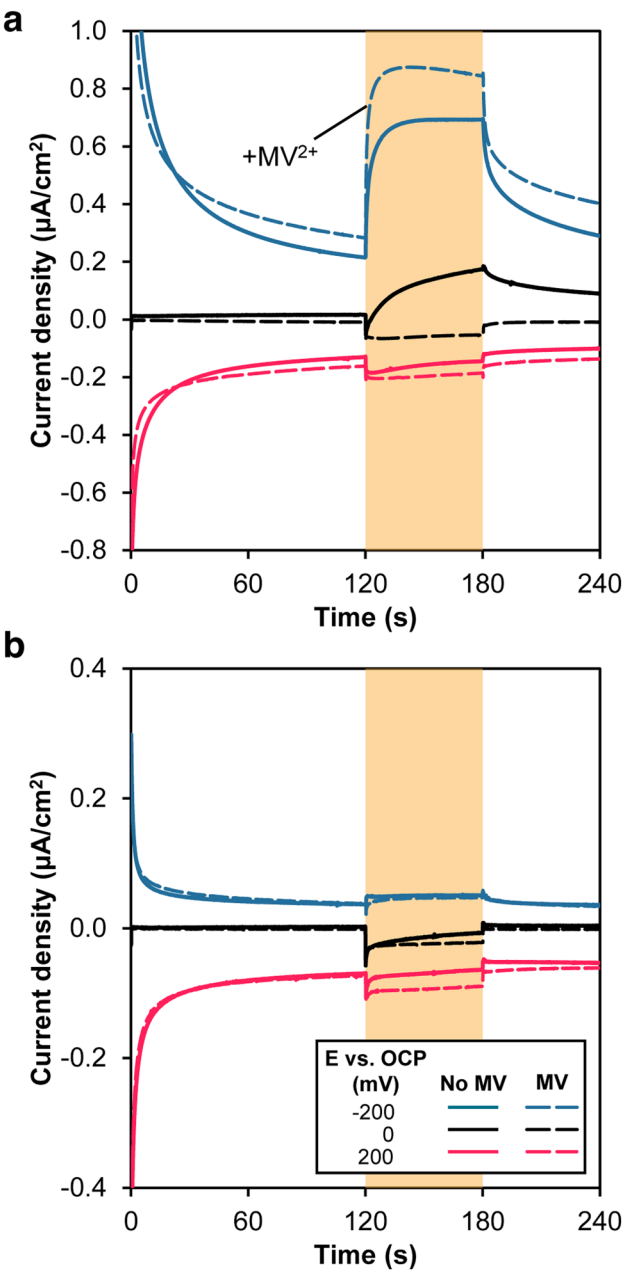


**Fig. 6** Photochronoamperometry experiments of (**a**) cyt c/PSI/Nafion (**b**) PSI/Nafion in 5 mM phosphate buffer (solid line) or 5 mM phosphate buffer and 250 µM methyl viologen (dashed line). Experiments were performed at OCP (black), −200 mV (blue), and + 200 mV (red) applied potentials relative to OCP. The sample was illuminated between 120 and 180 s

output of the cyt c/PSI/Nafion film is limited by the availability of electron acceptors to the $F_B$ site, and that there is potential to improve the performance of the system by incorporating electron mediators that are synergistic with cyt c. The PSI/Nafion film does not benefit as much from the presence of $MV^{2+}$ because, without cyt c, it is limited by the availability of electron donors to $P_{700}$ (Fig. 6b). In fact,

the PSI/Nafion film favors anodic photocurrent production and produces the highest photocurrent magnitude at positive bias, where the oxidation of mediator species at the electrode (ROS or $MV^+$) is kinetically favored. Likewise, when the cyt c/PSI/Nafion system is biased positive to decrease the availability of reduced cyt c, the addition of $MV^{2+}$ has a negligible effect due to the photocurrent being limited by the rate of $P_{700}^+$ reduction.

## Conclusion

We developed a rapid and simple drop-casting procedure to construct PSI-based photocathodes incorporating cyt c as an electron mediator and Nafion as a stabilizing top layer. Using only three drop-casting steps, we are able to achieve photoactive composite films with micron-scale thickness. The resulting film demonstrates the ability to entrap cyt c throughout the three-dimensional structure in a stable manner, which we attribute to electrostatic attraction between cyt c and the insoluble PSI and Nafion components of the film. Furthermore, the above configuration maintains cyt c diffusive mobility, which we show to be crucial to the ability of the film to mediate electron transfer to PSI that is distant from the electrode surface. The synergy between the ability of the drop-casted PSI film to retain cyt c and the ability of the retained cyt c to promote electron transfer to the $P_{700}^+$ site of PSI results in improved photocathodic current performance compared to the conventional drop-casted PSI multilayer film. Additionally, the photocurrent enhancement effect of cyt c is most apparent when a negative potential bias is applied. Further photocurrent enhancement is possible with the inclusion of a kinetically favorable electron mediator at the $F_B^-$ site such as $MV^{2+}$, which is not the case for the PSI film without cyt c. Our work not only confirms the compatibility of cyt c with PSI for improving the photocurrent performance of PSI-based devices, but also the drop-casting method as a way to achieve three-dimensional composite film architectures with minimal cost and processing effort. Looking forward, this work shows that efforts to better harness the redox capabilities of PSI and to improve the processability of PSI-based devices are both crucial to developing practical photoactive biohybrid technologies.

**Supplementary Information** The online version contains supplementary material available at https://doi.org/10.1007/s11120-022-00993-w.

**Acknowledgements** The authors would like to thank the United States Department of Agriculture (2019-67021-29857) and the Vanderbilt Undergraduate Summer Research Program (for L.T.) for funding this work, as well as the Vanderbilt Institute for Nanoscale Science & Engineering (VINSE) for the use of analytical instrumentation

**Funding** National Institute of Food and Agriculture, 2019-67021-29857, Kane Jennings, Vanderbilt University.

**Data Availability** Original data will be provided upon request.

## Declarations

**Conflict of interest** The authors have no financial or non-financial interests that are directly or indirectly related to this work submitted for publication.

## References

Aghamiri ZS, Mohsennia M, Rafiee-Pour H-A (2018) Immobilization of cytochrome c and its application as electrochemical biosensors. Talanta 176:195–207. https://doi.org/10.1016/j.talanta.2017.08.039

Baba K, Itoh S, Hastings G, Hoshina S (1996) Photoinhibition of Photosystem I electron transfer activity in isolated Photosystem I preparations with different chlorophyll contents. Photosynth Res 47:121–130. https://doi.org/10.1007/BF00016175

Badura A, Guschin D, Kothe T et al (2011) Photocurrent generation by Photosystem I integrated in crosslinked redox hydrogels. Energy Environ Sci 4:2435–2440. https://doi.org/10.1039/C1EE01126J

Baker DR, Simmerman RF, Sumner JJ et al (2014) Photoelectrochemistry of Photosystem I bound in nafion. Langmuir 30:13650–13655. https://doi.org/10.1021/la503132h

Balkenhohl Th, Adelt S, Dronov R, Lisdat F (2008) Oxygen-reducing electrodes based on layer-by-layer assemblies of cytochrome c and laccasse. Electrochem Commun 10:914–917. https://doi.org/10.1016/j.elecom.2008.04.007

Brettel K, Leibl W (2001) Electron transfer in Photosystem I. Biochim Biophys Acta (BBA) Bioenerg 1507:100–114. https://doi.org/10.1016/S0005-2728(01)00202-X

Chen X, Ferrigno R, Yang J, Whitesides GM (2002) Redox properties of cytochrome c adsorbed on self-assembled monolayers: a probe for protein conformation and orientation. Langmuir 18:7009–7015. https://doi.org/10.1021/la0204794

Chen G, LeBlanc G, Jennings GK, Cliffel DE (2013) Effect of redox mediator on the photo-induced current of a Photosystem I modified electrode. J Electrochem Soc 160:H315–H320. https://doi.org/10.1149/2.054306jes

Chitnis PR (2001) Photosystem I: function and physiology. Annu Rev Plant Physiol Plant Mol Biol 52:593–626. https://doi.org/10.1146/annurev.arplant.52.1.593

Ciesielski PN, Faulkner CJ, Irwin MT et al (2010) Enhanced photocurrent production by Photosystem I multilayer assemblies. Adv Func Mater 20:4048–4054. https://doi.org/10.1002/adfm.201001193

Ciornii D, Kölsch A, Zouni A, Lisdat F (2019) A precursor-approach in constructing 3D ITO electrodes for the improved performance of Photosystem I-cyt c photobioelectrodes. Nanoscale 11:15862–15870. https://doi.org/10.1039/C9NR04344F

Dervishogullari D, Gizzie EA, Jennings GK, Cliffel DE (2018) Polyviologen as electron transport material in Photosystem I-based biophotovoltaic cells. Langmuir 34:15658–15664. https://doi.org/10.1021/acs.langmuir.8b02967

Efrati A, Tel-Vered R, Michaeli D et al (2013) Cytochrome c-coupled Photosystem I and Photosystem II (PSI/PSII) photo-bioelectrochemical cells. Energy Environ Sci 6:2950–2956. https://doi.org/10.1039/C3EE41568F

Feifel SC, Ludwig R, Gorton L, Lisdat F (2012) Catalytically active silica nanoparticle-based supramolecular architectures of two

proteins – cellobiose dehydrogenase and cytochrome c on electrodes. Langmuir 28:9189–9194. https://doi.org/10.1021/la301290z

Ge B, Lisdat F (2002) Superoxide sensor based on cytochrome c immobilized on mixed-thiol SAM with a new calibration method. Anal Chim Acta 454:53–64. https://doi.org/10.1016/S0003-2670(01)01545-8

Gizzie EA, Scott Niezgoda J, Robinson MT et al (2015) Photosystem I-polyaniline/$TiO_2$ solid-state solar cells: simple devices for biohybrid solar energy conversion. Energy Environ Sci 8:3572–3576. https://doi.org/10.1039/C5EE03008K

Golbeck JH, Bryant DA (1991) Photosystem I. In: Lee CP (ed) Current Topics in Bioenergetics. Academic Press, Cambridge, pp 83–177

Grimme RA, Lubner CE, Bryant DA, Golbeck JH (2008) Photosystem I/molecular wire/metal nanoparticle bioconjugates for the photocatalytic production of $H_2$. J Am Chem Soc 130:6308–6309. https://doi.org/10.1021/ja800923y

Hahn CEW, Hill HAO, Ritchie MD, Sear JW (1990) The electrochemistry of proteins entrapped in nafion. J Chem Soc, Chem Commun. https://doi.org/10.1039/C39900000125

Kincaid HA, Niedringhaus T, Ciobanu M et al (2006) Entrapment of Photosystem I within self-assembled films. Langmuir 22:8114–8120. https://doi.org/10.1021/la061326+

Kölsch A, Hejazi M, Stieger KR et al (2018) Insights into the binding behavior of native and non-native cytochromes to Photosystem I from Thermosynechococcus elongatus. J Biol Chem 293:9090–9100. https://doi.org/10.1074/jbc.RA117.000953

Kothe T, Pöller S, Zhao F et al (2014) Engineered electron-transfer chain in Photosystem 1 based photocathodes outperforms electron-transfer rates in natural photosynthesis. Chem A Eur J 20:11029–11034. https://doi.org/10.1002/chem.201402585

Kraytsberg A, Ein-Eli Y (2014) Review of advanced materials for proton exchange membrane fuel cells. Energy Fuels 28:7303–7330. https://doi.org/10.1021/ef501977k

López-Bernabeu S, Huerta F, Morallón E, Montilla F (2017) Direct electron transfer to cytochrome c induced by a conducting polymer. J Phys Chem C 121:15870–15879. https://doi.org/10.1021/acs.jpcc.7b05204

Morlock S, Subramanian SK, Zouni A, Lisdat F (2021) Scalable three-dimensional photobioelectrodes made of reduced graphene oxide combined with Photosystem I. ACS Appl Mater Interfaces 13:11237–11246. https://doi.org/10.1021/acsami.1c01142

Nelson N, Ben-Shem A (2005) The structure of Photosystem I and evolution of photosynthesis. BioEssays 27:914–922. https://doi.org/10.1002/bies.20278

Oellerich S, Wackerbarth H, Hildebrandt P (2002) Spectroscopic characterization of nonnative conformational states of cytochrome c. J Phys Chem B 106:6566–6580. https://doi.org/10.1021/jp013841g

Sarauli D, Tanne J, Xu C et al (2010) Insights into the formation and operation of polyaniline sulfonate/cytochrome c multilayer electrodes: contributions of polyelectrolytes' properties. Phys Chem Chem Phys 12:14271–14277. https://doi.org/10.1039/c0cp00793e

Scheller W, Jin W, Ehrentreich-Förster E et al (1999) Cytochrome C based superoxide sensor for in vivo application. Electroanalysis 11:703–706. https://doi.org/10.1002/(sici)1521-4109(199907)11:10/11%3c703::aid-elan703%3e3.0.co;2-j

Shiozawa JA, Alberte RS, Thornber JP (1974) The P700-chlorophyll a-protein: isolation and some characteristics of the complex in higher plants. Arch Biochem Biophys 165:388–397. https://doi.org/10.1016/0003-9861(74)90177-5

Song S, Clark RA, Bowden EF, Tarlov MJ (1993) Characterization of cytochrome c/alkanethiolate structures prepared by self-assembly on gold. J Phys Chem 97:6564–6572. https://doi.org/10.1021/j100126a037

Spricigo R, Dronov R, Lisdat F et al (2009) Electrocatalytic sulfite biosensor with human sulfite oxidase co-immobilized with cytochrome c in a polyelectrolyte-containing multilayer. Anal Bioanal Chem 393:225–233. https://doi.org/10.1007/s00216-008-2432-y

Stieger KR, Feifel SC, Lokstein H, Lisdat F (2014) Advanced unidirectional photocurrent generation via cytochrome c as reaction partner for directed assembly of Photosystem I. Phys Chem Chem Phys 16:15667–15674. https://doi.org/10.1039/c4cp00935e

Stieger KR, Ciornii D, Kölsch A et al (2016a) Engineering of supramolecular photoactive protein architectures: the defined co-assembly of Photosystem I and cytochrome c using a nanoscaled DNA-matrix. Nanoscale 8:10695–10705. https://doi.org/10.1039/c6nr00097e

Stieger KR, Feifel SC, Lokstein H et al (2016b) Biohybrid architectures for efficient light-to-current conversion based on Photosystem I within scalable 3D mesoporous electrodes. J Mater Chem A 4:17009–17017. https://doi.org/10.1039/c6ta07141d

Teodor AH, Ooi E-J, Medina J, Alarcon M, Vaugh MD, Bruce BD, Bergkamp JJ (2021) Aqueous-soluble bipyridine cobalt(II/III) complexes act as direct redox mediators in Photosystem I-based biophotovoltaic devices. RSC Adv 11:10434–10450. https://doi.org/10.1039/D0RA10221K

Wolfe KD, Gargye A, Mwambutsa F et al (2021) Layer-by-layer assembly of Photosystem I and PEDOT:PSS biohybrid films for photocurrent generation. Langmuir 37:10481–10489. https://doi.org/10.1021/acs.langmuir.1c01385

Zhu W, Salles R, Miyachi M et al (2020) Photoelectric conversion system composed of gene-recombined Photosystem I and platinum nanoparticle nanosheet. Langmuir 36:6429–6435. https://doi.org/10.1021/acs.langmuir.0c00647